P. FIGIEL*#, D. GARBIEC**, A. BIEDUNKIEWICZ*, W. BIEDUNKIEWICZ***,
P. KOCHMAŃSKI*, R. WRÓBEL****

MICROSTRUCTURAL, CORROSION AND ABRASIVE CHARACTERISTICS OF TITANIUM MATRIX COMPOSITES

Commercially pure titanium is less expensive, generally more corrosion resistant and lower in strength than its alloys, and is not heat-treatable. The use of Ti and its alloys as construction materials under severe friction and wear conditions is limited due to their poor tribological properties. Nevertheless, proper addition of hard ceramic particles into Ti and its alloys has proved to be an efficient way to enhance their mechanical and wear properties. Our purpose in this work was to analyze the corrosion, tribocorrosion, mechanical and morphological effects of combining titanium carbide with titanium metal, to create a unique composite via spark plasma sintering technique (SPS). Composites with different mass percentage (1, 5, 10, 15 and 20 wt %) of ceramic phase were produced. The samples of pure Ti and Ti-6Al-4V alloy were also tested, as a reference. These composites were examined for mechanical properties and corrosion resistance in an environment similar to the human body (Ringer's solution). Open circuit potential (OPC) and anodic polarization measurements were performed. The properties of titanium composites reinforced with micro- and nanocrystalline TiC powders were compared. It was stated that wear properties were significantly improved with increasing amount of TiC in matrix, especially in the case of nanocrystalline reinforcement. In terms of corrosion resistance, the composites showed slightly worse properties compared to pure titanium and Ti-6Al-4V alloy.

Keywords: Titanium matrix composite, SPS, corrosion resistance, sliding wear

1. Introduction

Commercially pure titanium (cp-Ti) is less expensive, generally more corrosion resistant and lower in strength than its alloys, and is not heat-treatable. It is highly weldable and formable, and used primarily in applications requiring corrosion resistance and high ductility, where strength is not a prime consideration. These factors, make titanium as an attractive material for very wide range of applications. Corrosion resistance is guaranteed by a very dense layer of oxides, which in the event of damage is regenerated in the presence of oxygen-containing environments. Titanium oxide film also provides superior resistance to abrasion, erosion, erosion-corrosion, cavitation and impingement attack in high-velocity process streams. Low modulus of elasticity of the titanium means excellent flexibility and strong spring back characteristics. This promotes its use in various springs for aircraft and valves, where a modulus half that of steel, but a strength equivalent to steel allows a titanium spring to be half as large and heavy. This property also benefits car parts (which must absorb shock), medical implants (that must move with the body), architecture (where roofs must resist hail stones), as well

as recreational gear (golf clubs, tennis racquets, mountain bikes and skis). The percentage of titanium used in the global aerospace market increases with each design generation of aircraft [1].

The use of Ti and its alloys as construction materials under severe friction and wear conditions is limited due to their poor tribological properties [2-4]. However, according to literature survey, proper addition of hard ceramic particles with Ti and its alloys has proved to be an efficient way to enhance the mechanical and wear properties [5-7]. The thermo-mechanical and tribological properties of titanium also can be improved by reinforcing them with ceramics [8]. There is considerable interest in the development of Ti-based Metal Matrix Composites (MMCs) reinforced with high-stiffness ceramic particles. While offering an elevated-temperature resistant, ductile base, titanium can be further strengthened with the addition of ceramic compounds in fiber or particulate form to produce properties beyond those achieved by alloying alone. Titanium matrix composites have current applications such as industrial, automotive, and consumer [9]. Particulatereinforced titanium matrix composites are being considered for wear resistant (gears, bearings, shafts), erosion and corrosion resistant (tubing), and creep resistant (engine) applications [10].

* WEST POMERANIAN UNIVERSITY OF TECHNOLOGY, FACULTY OF MECHANICAL ENGINEERING AND MECHATRONICS, INSTITUTE OF MATERIALS SCIENCE AND ENGINEERING, 19 PIASTOW AV. 70-310 SZCZECIN, POLAND
** METAL FORMING INSTITUTE, 14 JANA PAWŁA II STR., 61-139 POZNAŃ, POLAND
*** WEST POMERANIAN UNIVERSITY OF TECHNOLOGY, FACULTY OF MECHANICAL ENGINEERING AND MECHATRONICS, INSTITUTE OF MANUFACTURING ENGINEERING, PIASTOW AV. 19, 70-310 SZCZECIN, POLAND
**** WEST POMERANIAN UNIVERSITY OF TECHNOLOGY, FACULTY OF CHEMICAL TECHNOLOGY AND ENGINEERING, INSTITUTE OF CHEMICAL TECHNOLOGY AND ENVIRONMENT ENGINEERING, 10 PUŁASKIEGO AV., 70-322 SZCZECIN, POLAND

\# Corresponding author: pfigiel@zut.edu.pl

The advantage of the composite materials is that their individual constituents retain their characteristic unlike alloys. As a result, various combinations of useful properties, usually not attainable by alloys, can be obtained through composite materials by suitable tailoring the matrix and reinforcement. Generally, metal matrix composites are used in wear applications, due to their high hardness while maintaining a reasonable level of toughness. The overall abrasion resistance is derived from the hard particles while the increase in toughness comes from the transition metal matrix. Wear resistance is one key aspect where the intrinsic properties of MMCs may be exploited. While there are many different types of wear, abrasion is one of the most ubiquitous modes found in industrial applications. A study by Van Acker et al. showed that when abrading using the ball-on-disc test an increased volume fraction of carbides with finer particle size were the most favorable conditions for minimizing wear in a WC-Ni MMC [11]. The other study by D. T. Cavanaugh showed that the effects of the titanium carbide differences in particle size on the abrasion resistance of steel matrix composite were noticeable. The particle morphology showed indications of influencing the wear mode, but no statistical reduction was observed in the volume loss figures. The most predominant effect in increasing abrasion resistance is confirmed to be volume fraction of titanium carbide addition [12]. As TiB/TiC are generally reported for high modulus, high thermal stability and chemical stability certain other similar investigations have endorsed improved wear resistance and much lower co-efficient of friction values for Ti/TiB and Ti/TiC MMCs [13].

In order to maximize interfacial bond strength in MMCs, it is necessary to promote wetting, control chemical interactions and minimize oxide formation. Adequate and coherent bonding between matrix and particles is essential to get maximum strength of the composites. The interfacial connection (consolidation of the composite) is possible through the chemical reaction between the matrix and the strengthening phase taking place in the sintering process. The particles and matrix react to the form of a new compound or compounds at the interface. They are responsible for the binding efficiency, and thus the consolidation of the composite, strength, low porosity and corrosion resistance. This approach guarantees a thermodynamically stable composite with clean interphase surfaces, well-consolidated, with maximum strength at low and elevated temperatures and fracture toughness. Composites attain their hardness and strength from strong chemical bonds, crystal structure and also from their nanostructure.

Ti-based MMCs are mainly prepared by powder metallurgy (PM), the casting solidification molding method, the spray molding method, and the laminated composite method [14-17]. For the base metal, a type and size of more than two kinds of second phase particles can be chosen according to the technical demands of the powder metallurgy composite method [18]. However, the reaction between the matrix metal and strengthening particles is hard to achieve through the traditional hot pressing process.

Spark plasma sintering (SPS) is a newly developed versatile technique to rapidly sinter powder materials in periods of minutes as compared to several hours required for conventional sintering. SPS involves simultaneous application of pressure and current directly on the powder materials. A high pulsed direct current is applied on the electrode and microscopic electrical discharges in the voids between powder particles generate a plasma, causing sintering. The main difference between SPS and other sintering methods is that in SPS both die and powder are directly heated by Joule effect of direct current [19].

Metal matrix composites have been widely studied in terms of abrasion resistance, but a particular material system may behave differently as particle size, morphology, composition, and distribution of the hardening phase varies. The purpose of this investigation was to understand the corrosion, abrasion-corrosion, mechanical and morphological effects of combining titanium carbide with titanium metal to create a unique composites via SPS. The properties of titanium composites reinforced with micro- and nanocrystalline TiC powders were compared. The effect of the presence of carbon cages on the surface of nanoparticles in the consolidation process of TiC and Ti on the properties of the Ti-based Matrix Nanocomposites was also analyzed. The tests were carried out for TiC/Ti composites, cp-Ti and commercial Ti-6Al-4V alloy samples.

2. Materials and methods

2.1. Preparation of Ti/TiC composites

In this work one type of cp-Ti (Grade 1), obtained by gas atomization from SLM Solutions GmbH, was employed as starting matrix material. Cp-Ti had a spherical shape and average particle size was around 100 μm (Fig. 1a). As a reinforcements two types of commercial titanium carbide particles from Sigma Aldrich were used: below 4 μm, (designated as μm-TiC), and below 200 nm (designated as nc-TiC). The microstructure of the particles is presented in Figure 1b and 1c, respectively. Additionally, the research applied a powder containing TiC in carbon cages (Fig. 1d) with an average crystallite size of 40 nm and ca 3 wt % elemental carbon content (designated as nc-TiC/C), obtained by a nonhydrolytic sol-gel method. The synthesis process, structure and morphology of nc-TiC/C powder were presented earlier [20].

The Ti with the TiC powders were milled in argon atmosphere using a planetary mill Pulverisette 4 (Fritsch GmbH), with use of the WC/Co milling balls in a weight ratio of 10:1 with respect to the powder. For sintering process the mixtures of the powders composed of 0, 1, 5, 10, 15 and 20 wt % of TiC and the titanium were used.

Spark plasma sintering (SPS) was used to study the effect of the size and presence of carbon cages on the surface of TiC particles distributed in titanium matrix in the consolidation process of TiC and Ti on the properties of the TiMMCs. For this purpose, an HP D 25-3 device FCT Systeme GmbH was used. The following parameters of the sintering process were used: sintering temperature – 1300°C, heating rate – 400°C/min,
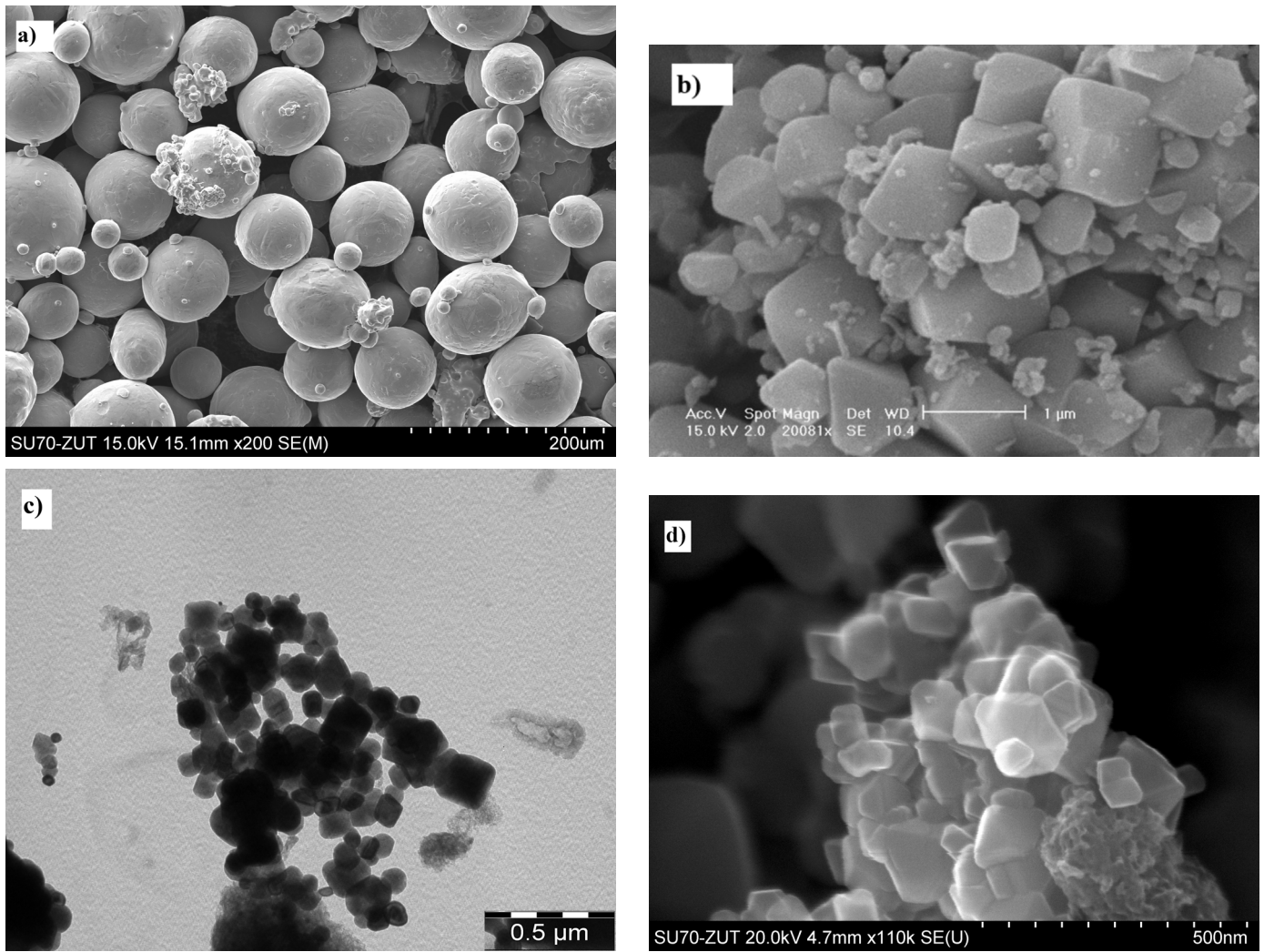
Fig. 1. Microstructure of starting material: a) Ti powder, b) μc-TiC c) nc-TiC, d) nc-TiC/C powders

sintering time – 2.5 min, press pressure – 50 MPa, vacuum level – 5 Pa. The samples obtained in the process had cylinder shape with a diameter of 20 mm and a height of 10 mm. A sample of the commercial Ti-6Al-4V alloy was cut from forged and rolled rod delivered from Bibus Metals company.

2.2. Structural characterization

Samples for XRD and XPS examination and tribocorrosion characterization were cut, then ground and polished using an ATM SAPHIR 550 grinder with a MD-Mezzo 220 disk and MD-Largo discs with the addition of 9 μm diamond suspension. Finishing step was carried out on MD-Chem disks using Al_2O_3 suspension with the addition of H_2O_2. For morphology investigation the second group of samples was sanded with 220 grit paper and electro-polished with Struers LectoPol-5 device, with the following parameters: 30-35 V voltage, 16 flow, 20 s time, 1 cm^2 surface and Struers A3 electrolyte.

The average size of crystallites in composites was measured by Scherrer and Debye-Hulla methods. The size of crystallites, morphology phase and chemical composition of the composites were determined with the following techniques: X-Ray diffraction (XRD) using PANalytical PW3040/60 X'Pert Pro apparatus equipped with Cu Kα radiation, light microscopy Nikon MM-40 with a Digital Sight DS-U1 camera in a bright field, with magnification: ×100, ×200 and ×500, scanning electron microscopy (SEM) using Hitachi SU-70 apparatus equipped with Thermo Fisher Noran 7 microanalysis adapter, transmission electron spectroscopy (TEM) using JEOL JEM 1200EX.

X-Ray Photoelectron spectroscopy (XPS) studies were carried out with use of the Prevac electron spectrometer, equipped with SES 2002 (VG Scienta) electron energy analyzer working in Constant Energy Aperture mode. Samples were exited with Al-Kα radiation ($h = 1489.6$ eV). The calibration was performed using a C 1 s carbon signal lying at 284.6 eV binding energy. The XPS test was carried out for composite samples with 20% nc-TiC/C, pure Ti and the Ti-6Al-4V alloy.

2.3. Mechanical and tribocorrosion tests

The Vickers hardness, HV, measurements were performed on Leco LM247AT indenter applying a 100 g load with an

indentation time of 10 s. Average hardness values of at least 10 measurements per sample were determined. Standard deviations did not exceed 10%. The density of the sintered samples was measured by Archimedes water immersion method.

Open-circuit corrosion potential (OCP) measurements were carried out in the separate cell for 240 min while potentiodynamic polarization measurements were performed using a scan rate of 0.01 V/s at a potential initiated at -1.0 V to $+1.5$ V. The measurement was carried out on the Atlas-Sollich 9833 potentiostat in a three-electrode system. The calomel (reference) and graphite (auxiliary) electrodes were used. The corrosion current calculations were performed using Tafel Slope Analysis. The analysis of the results has been carried out by means of the AtlasLab software. All corrosion tests were carried out in Ringer's solution, an electrolyte with a composition similar to extracellular fluid, simulating body fluids with a pH of 7.5. During the tests, the electrolytes were in natural oxygen containing state in room temperature.

The tribocorrosion (abrasion-corrosion) properties of the samples were studied using "ball-on-disk" technique. The tests were performed under ambient dry conditions on CSM tribometer (TRN model). Alumina ball with the diameter of 6 mm was slid on disc made of tested materials in rotating mode. The applied load was 3 N, and sliding distance of 500 m. Before each test, the specimens and balls were rinsed ultrasonically in acetone. DEKTAK 6M type profilometer (Veeco) was used to estimate the volume losses (V) and wear coefficient (K).

3. Results and discussion

The X-ray diffraction patterns are used to analyze the phase composition of the samples and are shown in Figures 2 and 3. Figure 2 shows X-ray diffraction spectra of the titanium carbide phase in the carbon cages. The broad peak at 25.34° can be attributed to carbon (002), and the other five sharp peaks at 36.21° (111), 42.06° (200), 60.99° (220), 73.04° (311) and 76.86° (222) can be well assigned to TiC [19]. Figure 3 shows X-ray diffraction patterns of the Ti powder after sintering process. The example of XRD patterns of the titanium matrix composites containing respectively 1, 5, 10, 15 and 20 wt % TiC are presented in Figures 4.
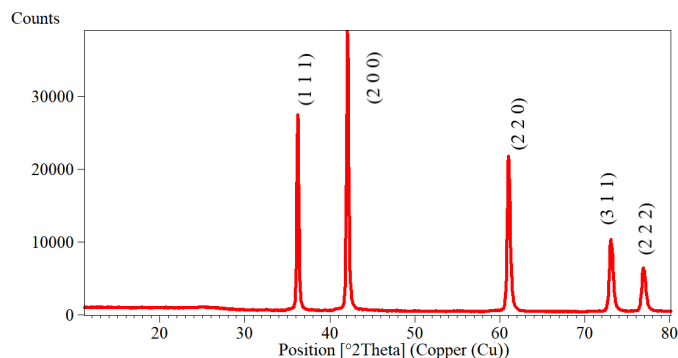

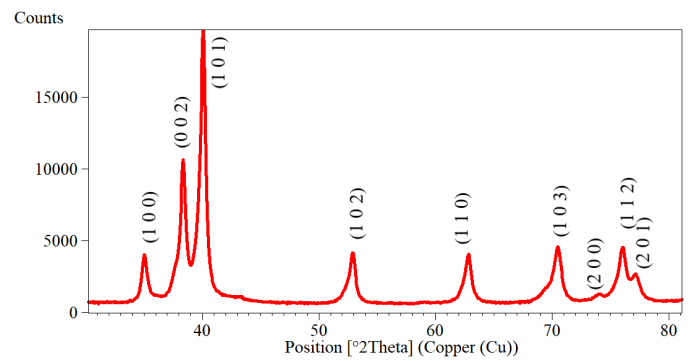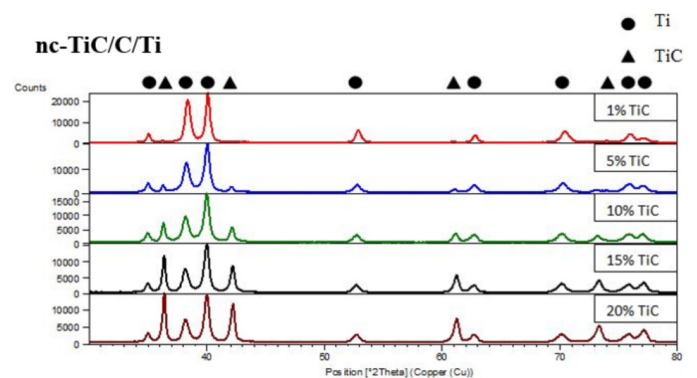Fig. 2. X-Ray diffraction pattern of the nc-TiC/C powder

Fig. 3. X-Ray diffraction pattern of the titanium after sintering process via SPS

Fig. 4. Comparison of X-Ray diffraction patterns of the titanium matrix with the increase in the proportion of titanium carbide in the nc-TiC/C/Ti composites

Analyzing the results of X-ray diffraction tests, there is a change in the intensity distribution of interference reflections of the titanium matrix with the increase in the proportion of titanium carbide in the composites (Fig. 4). The I_{101}/I_{002} of Ti peak's ratio in composite samples are not the same as the data in JCPDS card. This indicates that in all of composite samples Ti phase possess texture. During the spark plasma sintering process (SPS) the titanium crystallites are oriented from random to anisotropic. The largest deviations from the random orientation were observed in composites containing 1% of TiC. Together with the increase in TiC content in titanium composites, the ratio of intensity of diffraction lines of titanium d_{101}/d_{002} increases, suggesting a change in the orientation of titanium crystallites from anisotropic to random. In all examined composites, a higher intensity of the d_{111} diffraction line was observed compared to the d_{200} line, which indicates the texture of titanium carbide (TiC) in the titanium matrix, probably resulting from the SPS sintering method. Changes in the orientation of the TiC crystallites in the titanium matrix together with the change in the TiC content were not observed.

The micrographs illustrated in figures 5 and 6 give evidence for the distribution of reinforcements in the matrix. These results showed that the strengthening phase was located inter-crystalline in the structure of composites.

In the case of the nc-TiC/C/Ti nanocomposite, the ratio of intergranular areas to areas of the titanium matrix is larger
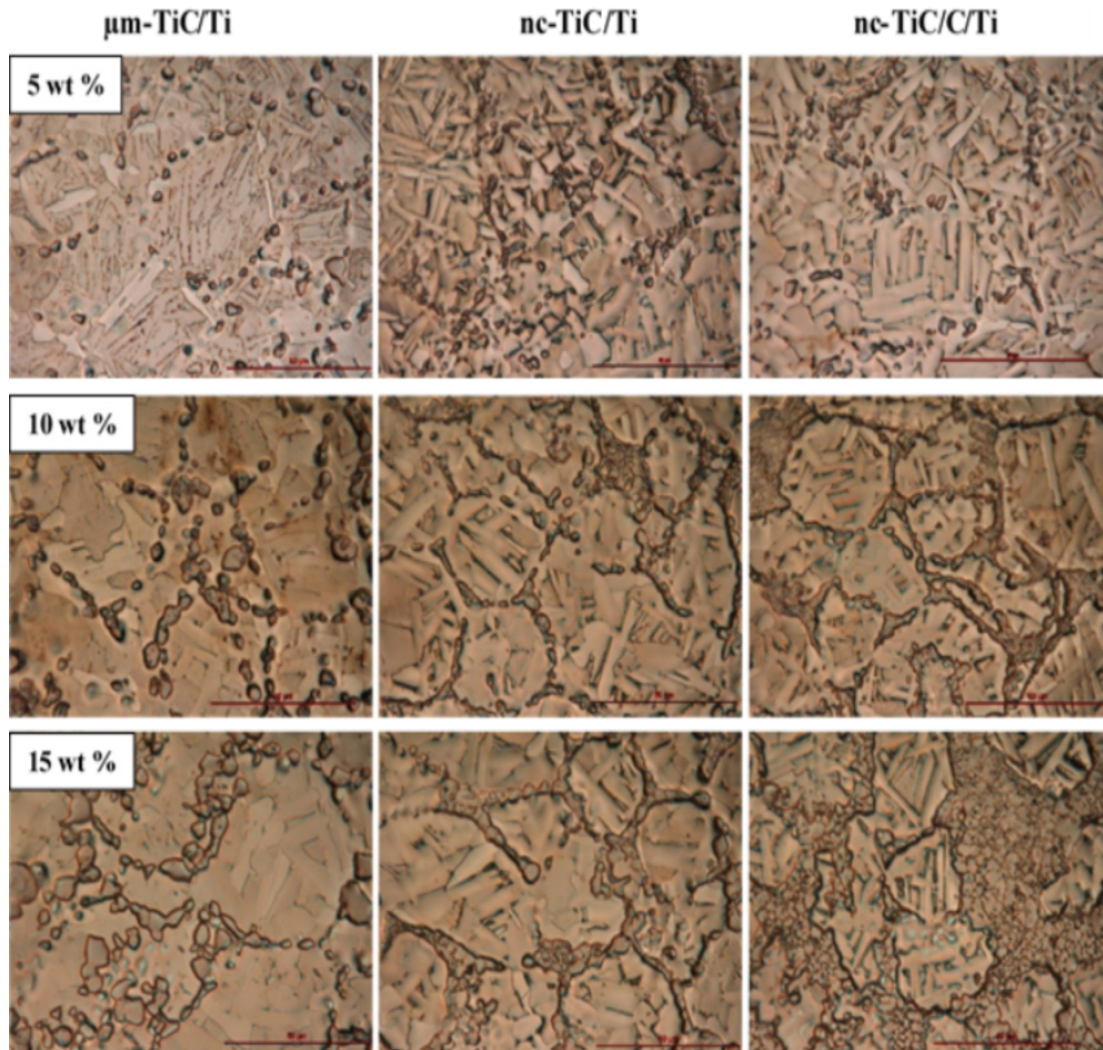
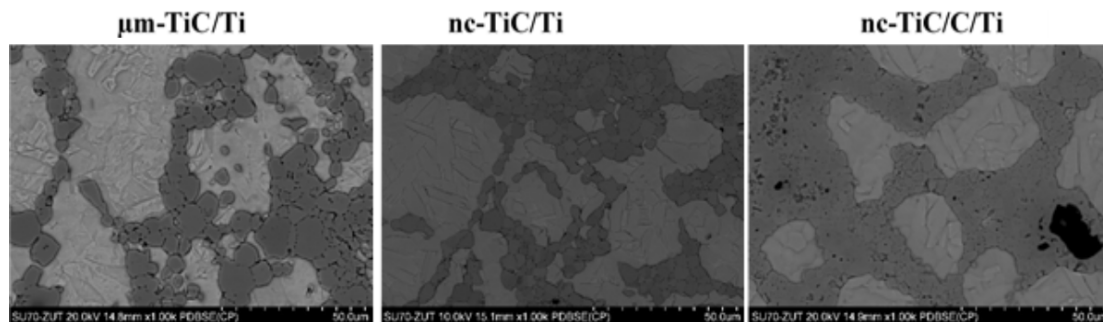Fig. 5. Light micrographs of electropolished TiMMCs samples containing 5, 10 and 15 wt % of TiC

Fig. 6. SEM images of electropolished TiMMCs samples containing 20 wt % of TiC

compared to the other composites. The size of the titanium crystallites has decreased. The decrease in the proportion of metallic titanium in this composite is also suggested by the results of XRD research (Fig. 4), which shows a comparison of the intensity of the strongest interference reflections of Ti and TiC for all composites containing 20 wt % TiC.

Density of the TiC reinforcement (4.92 g/cm^3) compared to the of pure titanium (4.507 g/cm^3) is similar, therefore changes in the relative density of composites should be attributed to their porosity (Fig. 7). Among the composites, the nc-TiC/C/Ti

composites showed the highest density, with the exception of a composite containing 20 wt % nc-TiC/C. In the structure of this particular nc-TiC/C/Ti composite, carbon grains were observed incidentally (Fig. 6). This is the result of insufficient conversion of free carbon with the titanium matrix material.

The graph on Fig. 8 demonstrates the values of hardness with respect to reinforcing quantity of TiC.

A comparison of the tribocorrosion test results of SPS-processed Ti/TiC composites are shown in Fig. 9a and 9b. It was observed that the volume losses (V) and wear coefficient
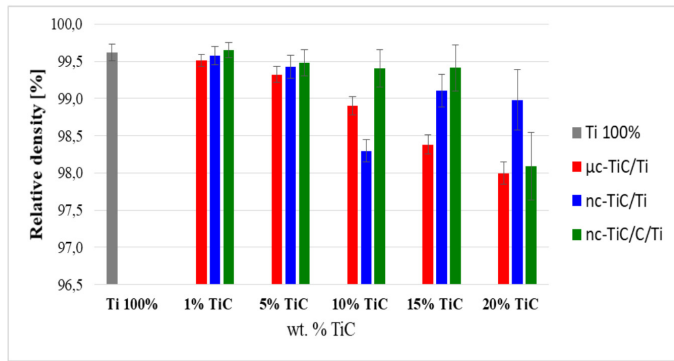
Fig. 7. Comparison of relative density values of TiC/Ti composites with different TiC content
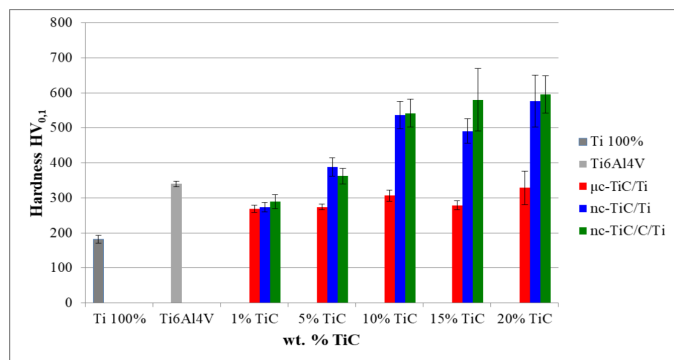

Fig. 8. Hardness of the composites with respect to reinforcing quantity of TiC and reference samples of pure Ti and Ti-6Al-4V

(K) decreased with the mass fraction of TiC in titanium matrix from 0 to 20 wt %. The best tribocorrosion resistance under ambient dry conditions was observed for the nc-TiC/C/Ti (20 wt %) nanocomposite.
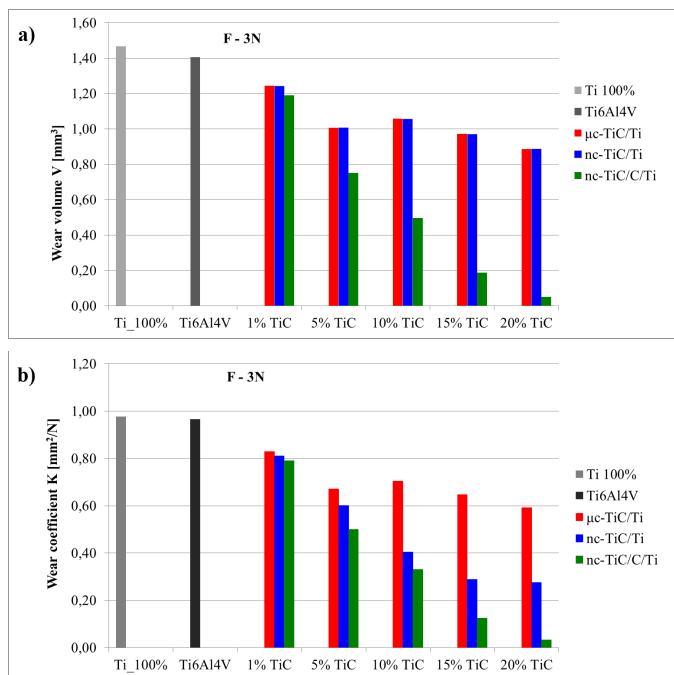

Fig. 9. Comparison of wear volume (a) and wear coefficient (b) for TiC/Ti composites, pure Ti and Ti-6Al-4V alloy

The variation in the open circuit potentials (OCP) of the produced composites exposed to Ringer solution after polishing is presented in Figure 10.
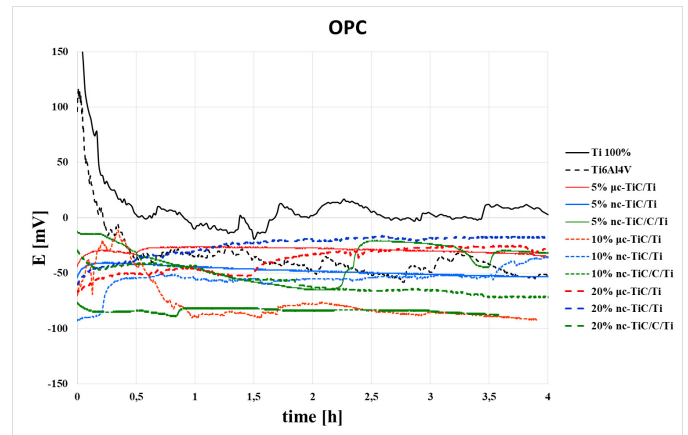

Fig. 10. The variation in the OCP of the composites exposed to Ringer solution

It is observed from Fig. 10 which presents the OCP profile of the composites containing 1, 10 and 20 wt % of TiC reinforcement that the open circuit potentials for Ti, Ti-6Al-4V and some composite samples fluctuate continuously. The exception is observed in case of composites containing 10 and 20 wt % of nc-TiC, 10 and 20 wt % of nc-TiC/C and 5 wt % of μc-TiC which had a fairly stable OCP profile. The fluctuation of OCP values in the manner observed in these composites is typical for materials systems undergoing repeated passive film formation and breakdown due to exposure to a corrosive environment.

From the OCP profiles of the composites in this tests, it is noted that the nc-TiC/Ti (20 wt %) composite had the highest open circuit potential in comparison with the other Ti composite. This suggests that the nc-TiC/Ti (20 wt %) composite will have the least thermodynamic tendency to corrode in the Ringer solution. It also appears that the OCP profiles of the nc-TiC/Ti (10 wt %), μc-TiC/Ti (5 and 10 wt %) and nc-TiC/C/Ti (5 wt %) composites are shifted to higher values compared to the Ti-6Al-4V alloy and other composites. The OCP profiles of the nc-TiC/C/Ti (10 and 20 wt %) composites are shifted to lower values but they are characterized by a constant value of the open circuit potential in time. The OCP profile of the nc-TiC/C/Ti (5 wt %) composite is shifted to higher values but the open circuit potentials for these composites fluctuate periodically. This means a higher thermodynamic stability and hence a lesser tendency to corrode in Ringer solution in comparison with the other nc-TiC/C/Ti composites. From among the nc-TiC/Ti composites the OCP profiles of the nc-TiC/Ti (5 and 20 wt %) composites are characterized by a constant value of potential in time. Comparing μc-TiC/Ti composites the OCP profile of the composite containing 1 wt % of μc-TiC is characterized by a constant value of potential in time. In other cases of OCP measurements, fluctuations in potential observed in time were caused by the reconstruction of the oxide layer in the passivation process.

The potentiodynamic polarization curves for the composites in Ringer solution (Fig. 11) help in analyzing more thoroughly the corrosion behavior of the composites. Figure 11 shows that the composites generally displayed similar polarization curves and passivity characteristics. However, the corrosion potentials (E_{corr}) of the composites were clearly distinct and occurred in the ranges of −0.091 to −0. 351 V. Table 1 which presents the corrosion potential (E_{corr}) and corrosion current density (I_{corr}) data of all the composites produced was obtained from Fig. 11. On analysis of the composites in this tests, it is noted that the corrosion potentials (E_{corr}) and corrosion current density (I_{corr}) of the μc-TiC/Ti composites exhibit a constant trend of changes in value along with a change in the TiC content. It is clearly seen that E_{corr} and corrosion I_{corr} of the nc-TiC/Ti and nc-TiC/C/Ti nanocomposites did not follow a consistent trend with variation in the weight percent of reinforcement phase.

In case of pure Ti sintered sample immersed in Ringer solution, corrosion potential was at the level of −0.098 V and corro-

sion current density reached $3.19 \cdot 10^{-6}$ A·cm^{-2}. When 1÷20% TiC Ti-based MMCs are immersed in Ringer solution, the corrosion potential generally shifts from -0.098 V to lower values towards cathodic region. The exception is observed in case of composites containing 10 wt % nc-TiC/C. Together with the increase in μc-TiC content in μc-TiC/Ti microcomposites, the corrosion potential shifted from −0.351 V to higher values towards anodic region, and corrosion current density increased from $0.785 \cdot 10^{-6}$ to $7,82 \cdot 10^{-6}$ Acm^{-2}. This possible increase in corrosion current is an indication for low corrosion resistance of the μc-TiC/Ti microcomposite tested. This trend was not observed in the case of nanocomposites. Nanocomposites containing 10 wt % nc-TiC/C or containing 10 wt % nc-TiC had the highest values of corrosion potentials and the lowest corrosion current densities (Tab. 1). The results of these tests are not consistent with the observations of the OCP profiles. The deterioration of the corrosion resistance of nanocomposites with 20 wt % nc-TiC content was probably due to the increase in their porosity. The nc-TiC/C/Ti (10 wt %) and nc-TiC/Ti (10 wt %) nanocomposites and additionally μc-TiC/Ti (1 wt %) microcomposite were characterized by the best corrosion resistance which is measured by the relatively higher resistance polarization (R_{pol}) values.

TABLE 1

Corrosion parameters in Ringer solution

Material	$E_{corr,}$ [V]	i_{corr} [A/cm^2]	R_{pol} [Ω/cm^2]
100% Ti 2018	−0,098	$3,19 \cdot 10^{-6}$	$9,19 \cdot 10^3$
Ti-6Al-4V rod	−0,426	$22,40 \cdot 10^{-6}$	$1,31 \cdot 10^3$
1% μc-TiC/Ti	−0,351	$0,785 \cdot 10^{-6}$	$42,87 \cdot 10^3$
10% μc-TiC/Ti	−0,267	$2,33 \cdot 10^{-6}$	$15,22 \cdot 10^3$
20% μc-TiC/Ti	−0,221	$7,82 \cdot 10^{-6}$	$5,87 \cdot 10^3$
1% nc-TiC/Ti	−0,304	$3,91 \cdot 10^{-6}$	$10,58 \cdot 10^3$
10% nc-TiC/Ti	−0,158	$1,02 \cdot 10^{-6}$	$43,95 \cdot 10^3$
20% nc-TiC/Ti	−0,226	$5,34 \cdot 10^{-6}$	$6,84 \cdot 10^3$
1% nc-TiC/C/Ti	−0,304	$1,96 \cdot 10^{-6}$	$13,77 \cdot 10^3$
10% nc-TiC/C/Ti	−0,091	$1,42 \cdot 10^{-6}$	$33,06 \cdot 10^3$
20% nc-TiC/C/Ti	−0,218	$5,72 \cdot 10^{-6}$	$6,15 \cdot 10^3$

The corrosion mechanism in titanium, titanium alloy and Ti-based MMCs is mainly attributed to the fact that compact and stable oxide passive films can be formed on the material surface. The titanium, titanium alloy and nc-TiC/C/Ti (20 wt %) samples have also been analyzed by XPS method. The XPS characteristic lines of oxygen, titanium and carbon are shown in Figures 12-14. Fig. 12 displays exemplary O 1 s spectra recorded at ca. 530 eV and above 532 eV. The binding energy around the value of approximately 530 eV corresponds to TiO$_2$, while the binding energy values above 532 eV could be assigned to Ti-O-H in the case of titanium and titanium composite and to Al$_2$O$_3$ or also Al-O-H in the case of Ti alloy [21-24].

Fig. 13 displays exemplary Ti 2p$_{3/2}$ and Ti 2p$_{1/2}$ spectra recorded at ca. 459 eV and above 464 eV. The literature values of binding energies for TiO2 compound are about 458.5 and 464.3 eV, respectively [25]. The XP spectra are virtually identi-
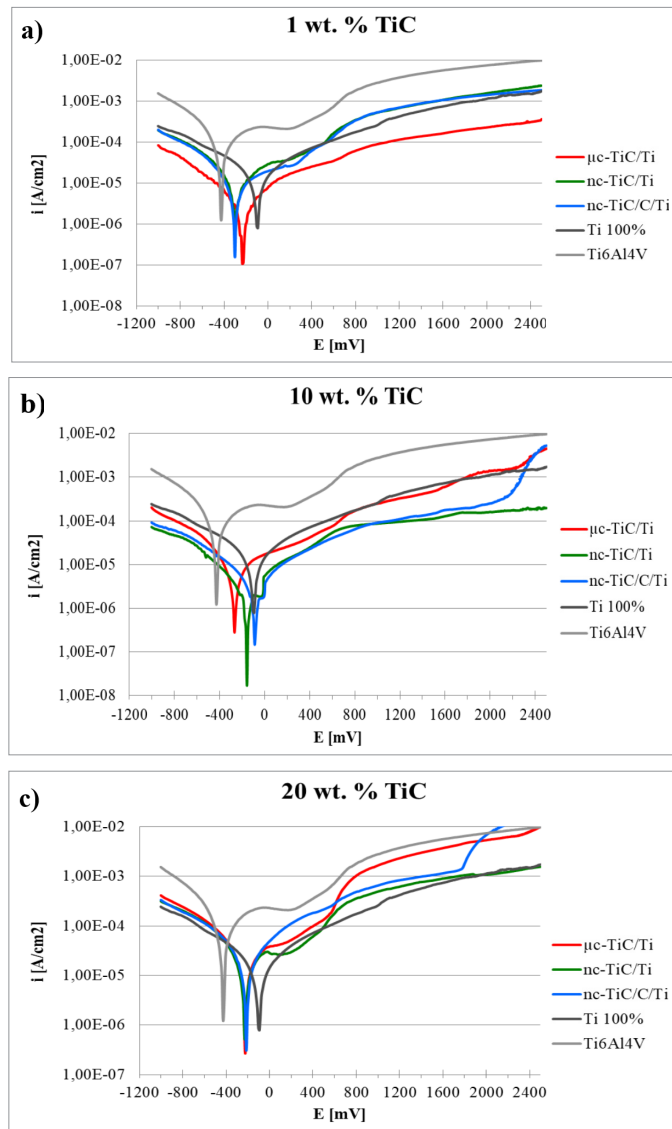
Fig. 11. Comparison of anodic polarization curves of pure Ti, Ti-6Al-4V alloy and TiC/Ti composites, a) 1 wt %, b) 10 wt% and c) 20 wt% of TiC in the Ti matrix

cal for both of Ti and Ti composite samples. The binding energy corresponding to Ti 2p spectra of TiO_2 on nc-TiC/C/Ti (20 wt %) are shifted by about 0.5 eV towards higher values and could be attributed to the TiO_2 identified on the surface of pure titanium. This is most likely caused by the presence of carbon from the strengthening phase occurring in the titanium matrix. The lower intensity of Ti $2p_{3/2}$ and Ti $2p_{1/2}$ signal in case of Ti6Al4V sample is a result of much lower concentration of titanium in the alloy compared to other samples. The low intensity cannot be explained by thinner layer of TiO_2 because of absence of Ti 2p signal at 454 eV and 460 eV which is expected for metallic titanium [25]. Therefore the TiO_2 film is thick enough to completely attenuate signal from metallic titanium.
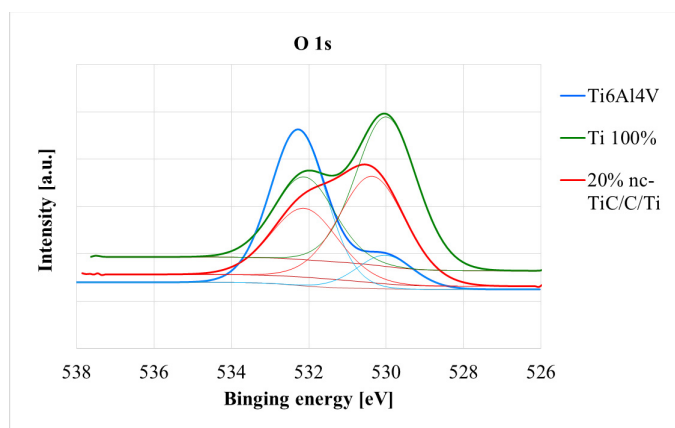

Fig. 12. XPS spectra of oxygen O1s of the pure Ti, Ti-6Al-4V alloy and the nc-TiC/C/Ti (20wt %) nanocomposite
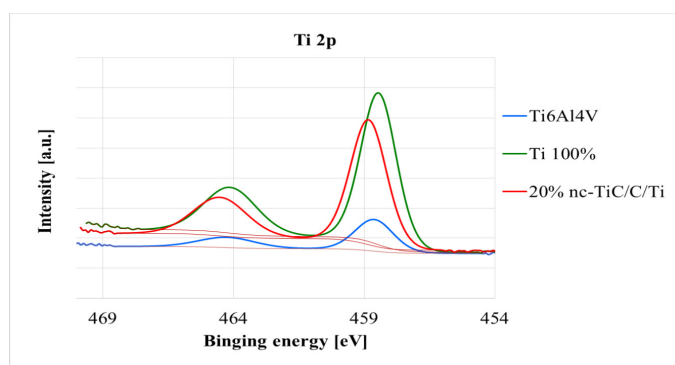

Fig. 13. Ti $2p_{3/2}$ and Ti $2p_{1/2}$ spectra of the pure Ti, Ti-6Al-4V alloy and the nc-TiC/C/Ti (20wt %) nanocomposite

In Fig. 14 there are presented C1s XP spectra.

One can expect carbon signal from TiC compound. It should be present at binding energies 281.9-282.0 ev [26]. Its absence may be explained by screening effect of carbon overlayer on the surface. A thin layer of carbonaceous material is usually found on the surface of most air exposed samples, this layer is generally known as adventitious carbon. Therefore is commonly used as a reference in calibration in XPS technique. This contamination may appear even in the vacuum conditions over the initially clean sample both due to decomposition of residual hydrocarbons and CO or through segregation of carbon to the surface from bulk [27].
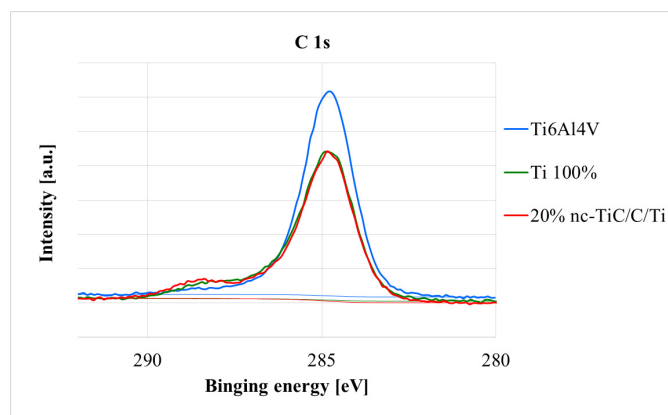

Fig. 14. C 1s spectra of pure Ti, Ti-6Al-4V alloy and nc-TiC/C/Ti (20 wt %) nanocomposite

The C1s signal consist of adventitious carbon 284.6 ± 0.3 eV and carbon-oxygen groups: C = O 287.6 ± 0.3 eV, C-O, 286.1 ± 0.3 eV, COOH 289.1 ± 0.3 eV, keto-enolic 286.4 ± 0.3 eV [28]. One can conclude that carbon over the surface of pure Ti samples and 20%nc-TiC/C/Ti composite have more oxygen-carbon groups compared to Ti6Al4V sample.

4. Conclusion

In this study, results of investigation on SPS-processed bulk-form titanium (Ti) and TiC/Ti micro- and nanocomposites in comparison with the Ti-6Al-4V alloy were presented. The TiC reinforcement is intergranularly distributed in the Ti matrix. The results showed that the strengthening phase was located inter-crystalline in the structure of composites. In the case of the nc-TiC/C/Ti nanocomposite, the ratio of intergranular areas to areas of the titanium matrix is larger compared to the other composites. The decrease in the titanium content with respect to the strengthening phase in this composite suggests the possibility of reaction of titanium with carbon, which was a coating on the surface of nc-TiC. There was observed the TiC nanocrystals growth from 40 to 90 nm in Ti matrix during SPS process. The relative density values of all TiC/Ti composites was high above 98%. Among the composites, the nc-TiC/C/Ti composites showed the highest density, with the exception of a composite containing 20 vol. % nc-TiC/C. In the structure of this particular nc-TiC/C/Ti composite, carbon grains were observed incidentally. This is the result of insufficient conversion of free carbon with the titanium matrix material. In all of the TiMMCs Ti phase possess texture. During the spark plasma sintering process (SPS) the titanium crystallites are oriented from random to anisotropic. The largest deviations from the random orientation were observed in composites containing 1% of TiC. Together with the increase in TiC content in titanium composites the orientation of titanium crystallites changed from anisotropic to random. There was indicated the texture of titanium carbide (TiC) in the titanium matrix, probably resulting from the SPS sintering method. Changes in the orientation of the TiC crystal-

lites in the titanium matrix together with the change in the TiC content were not observed. The hardness of composites containing 1% TiC is higher than the hardness of titanium and clearly lower than the hardness of the Ti-6Al-4V alloy. The composites achieved higher hardness than the Ti-6Al-4V alloy with 10 and 20 wt % TiC. The nc-TiC/C/Ti nanocomposite containing 20 wt % nc-TiC/C showed a 2-fold increase in hardness compared to the μc-TiC/Ti composite with the same TiC content. It is a matter of fact that reinforcements hinder the dislocation motion during plastic deformation equable for hardness improvement. The nc-TiC/C/Ti (20 wt %) nanocomposite was characterized by the best tribocorrosion resistance under ambient dry conditions. The potentiodynamic measurements of polarization in Ringer's solution helped in an accurate analysis of the corrosion behavior of TiMMCs sinter and comparison with the cp-Ti sinter obtained by the SPS method and a solid Ti-6Al-4V alloy. Along with the increase in μc-TiC content, the corrosion resistance of μc-TiC/Ti microcomposites decreases. This trend was not observed in the case of nanocomposites. The highest corrosion resistance was observed for nanocomposites containing 10 wt % of nc-TiC/C or containing 10 wt % of nc-TiC. The results of these tests are not consistent with the observations of the OCP profiles. The deterioration of the corrosion resistance of nanocomposites with 20 wt% nc-TiC content was probably due to the increase in their porosity. The nc-TiC/C/Ti (10 wt %) and nc-TiC/Ti (10 wt %) nanocomposites and additionally μc-TiC/Ti (1 wt %) microcomposite were characterized by the best corrosion resistance which is measured by the relatively higher resistance polarization (R_{pol}) values. The XPS spectra are virtually identical for both of cp-Ti sinter and TiC/Ti composite sinter samples. The binding energy corresponding to Ti 2p spectra of TiO_2 on nc-TiC/C/Ti (20 wt %) is shifted by about 0.5 eV towards higher values and equals to the TiO_2 identified on the surface of pure titanium. This is most likely caused by the presence of carbon from the strengthening phase occurring in the titanium matrix. Comparison of the intensity ratio of the Ti $2p_{3/2}$ and Ti $2p_{1/2}$ peaks suggests that a much thinner layer of TiO_2 was formed on the surface of the solid Ti-6Al-4V alloy in comparison to cp-Ti sinter and the nc-TiC/C/Ti (20 wt %) composite sinter.

REFERENCES

[1] http://c.ymcdn.com/sites/www.titanium.org/resource/resmgr/Docs/TiUltimate.pdf, accessed: 03.04.2018r.

[2] Y. S. Tian, C. Z. Chen, L. B. Chen, J. H. Liu, T. Q. Lei, J. Mater. Sci. **40**, 4387-4390 (2005).

[3] Marc Long, H.J. Rack, Wear **249**, 157-167 (2001).

[4] S. Fouvry, C. Paulin, S. Deyber, Tribol. Int. **42**, 461-474 (2009).

[5] D. E. Alman, J. A. Hawk, Wear **225-229**, 629-639 (1999).

[6] H. O. Gülsoy, V. Gunay, T. Baykara, Powder Metall. **58** (1), 30-35 (2015).

[7] A. A.M. da Silva, A. Meyer, J. F. dos Santos, C. E. F. Kwietniewski, T. R. Strohaecker, Compos. Sci. Technol. **64**, 1495-1501 (2004).

[8] C. Poletti, M. Balog, T. Schubert, V. Liedtke, C. Edtmaier, Compos. Sci. Technol. **68** (9), 2171-2177 (2008).

[9] N. Takahashi, T. Sato, S. Nakatsuka, K. Fujiwara, K. Yokozekii, Titanium metal matrix composite development for commercial aircraft landing gear structure, Proceedings of 28th International Congress of The Aeronautical Sciences 2012, Brisbane, Australia, (2012).

[10] L. Cai, Y. Zhang, L. Shi, H. Yang, M. Xi, J. Univ. Sci. Technol. Beijing Miner. Metall. Mater. (Eng Ed), **13** (6), 551-557 (2006).

[11] K. Van Acker, D. Vanhoyweghen, R. Persoons, J. Vangrunderbeek, Wear **258** (1-4), 194-202 (2005).

[12] D. T. Cavanaugh, Graduate Theses and Dissertations, Evaluation of titanium carbide metal matrix composites deposited via laser cladding, Iowa State University, Ames, USA (2015).

[13] Y. L. Qin, L Geng, D. R. Ni, J. Compos. Mater. **46** (21), 2637-2645 **(**2012).

[14] K. Mizuuchi, K. Inoue, M. Sugioka, M. Itami, M. Kawahara, I. Yamauchi, Mater. Sci. Eng. A **428**, 175-179 (2006).

[15] J.E. Oghenevweta, D. Wexler, A. Calka, J. Alloys Compd. **701**, 380-391 **(**2017).

[16] M.J. Bermingham, D. Kent, H. Zhan, D.H. StJohn, M.S. Dargusch, Acta Mater. **91**, 289-303 (2015).

[17] S. Roy, S. Suwas, S. Tamirisakandala, D.B. Miracle, R. Srinivasan, Acta Mater. **59**, 5494-5510 (2011).

[18] M. Sherif El-Eskandarany (Ed.), Mechanical Alloying: Nanotechnology, Materials Science and Powder Metallurgy, Wiliam Andrew Publishing, Oxford (2015)

[19] R. Chaudhari, R. Bauri, Metallogr. Microstruct. Anal. **3**, 30-35 (2014).

[20] A. Biedunkiewicz, J. Sol-Gel. Sci. Technol. **59**, 448-455 (2011).

[21] http://www.specs.de/cms/upload/PDFs/ApplNotes/Focus_500/ANote_xps_Ti_Al_V.pdf accessed 24.04.2018

[22] http://www.xpsfitting.com/2008/09/aluminum.html, accessed 25.04.2018

[23] D. E. MacDonald, B. E. Rapuano, H. C. Schniepp, Colloids Surf., B **82** (1), 173-181 (2011).

[24] D. Kuscer, J. Kovač, M. Kosec, R. Andriesen, J. Eur. Ceram. Soc. **28**, 577-584 (2008).

[25] M.C. Biesinger, L.W.M. Lau, A.R. Gerson, R.S.C Smart, Appl. Surf. Sci. **257**, 887-898 (2010).

[26] M. Magnuson, E. Lewin, L. Hultman, U. Jansson, Phys. Rev. B **80**, 235108 (2009).

[27] R.J. Wróbel, S. Becker, Vacuum **84**, 1258-1265 (2010).

[28] A. Gęsikiewicz-Puchalska, M. Zgrzebnicki, B. Michalkiewicz, U. Narkiewicz, A.W. Morawski, R.J. Wróbel, Chem. Eng. J. **309**, 159-171 (2017).